Brazilian Journal of Physics (2024) 54:66
https://doi.org/10.1007/s13538-024-01438-6

An Insight Into the Dynamics of Carreau-Yasuda Nanofluid Through a Wavy Channel with Electroosmotic Effects: Relevance to Physiological Ducts

A. Abbasi[1] · W. Farooq[1] · Sami Ullah Khan[2] · Adnan[3] · Arshad Riaz[4] · M. M. Bhatti[5,6]

Received: 14 December 2023 / Accepted: 9 February 2024 / Published online: 26 February 2024

Abstract
Many physiological ducts, like sperm vessels, intestines, common bile ducts, ducts of salivary glands, and ducts in the repertory system, are common ducts in which transport occurs due to the propagation of complex waves on the boundary. Electroosmotic flow phenomena are significant in membrane separation processes, protein and peptide delivery, iontophoresis in drug delivery through physiological ducts, and a lot of application in plant physiology regarding pressure control in xylem and phloem vessels. The aim of this theoretical study is to analyze the thermal characteristics of physiological fluid characterized by the Carreau-Yasuda model in a complex wavy channel. The two agents of flow, i.e., the propagation of complex waves on the walls of the channel and the electric field in the axial direction, are considered. Different zeta potentials at both walls of the asymmetric channel are employed. Basic conservation laws, along with the Poisson-Boltzmann equation, are utilized to model the problem in the Cartesian coordinate system. Theoretical and biological assumptions like greater wavelength, lubrication transport, and Debye-Hückel linearization transform the governing equations of PDE into a coupled system of ODE. The shooting method is used, which is Solve, a built-in function in the computational software Mathematica to compute the stream function, temperature profile, concentration profile, and various flow and heat transfer characteristics. The impact of various penetrating parameters is described through plots. The magnitude of the velocity profile is increased near the center of geometry by increasing the electroosmotic parameter in the lower half of the regime. Then the Sherwood number and the Bejan number show enhanced behavior by increasing the electroosmotic parameter. The current analysis predicts dynamic applications in thermodynamical systems, cooling systems, biochemistry, and drug delivery systems.

Keywords Entropy generation · Nanofluid · Carreau-Yasuda fluid model · Electro-osmosis · Complex wavy channel · Joule heating · Different zeta potentials

✉ M. M. Bhatti
mmbhatti@sdust.edu.cn

1 Department of Mathematics, University of Azad Jammu and Kashmir Muzaffarabad, Muzaffarabad 13100, Pakistan

2 Department of Mathematics, Namal University, Mianwali 42250, Pakistan

3 Department of Mathematics, Mohi-Ud-Din Islamic University, Nerian Sharif 12080, AJ&K, Pakistan

4 Division of Science and Technology, Department of Mathematics, University of Education, Lahore 54770, Pakistan

5 College of Mathematics and Systems Science, Shandong University of Science & Technology, Qingdao 266590, China

6 Material Science Innovation and Modelling (MaSIM) Research Focus Area, North-West University (Mafikeng Campus), Private Bag X2046, Mmabatho 2735, South Africa

Nomenclature

$e_i, i = 1, 2, 3, 4$	Amplitude of the peristaltic wave
T'	Averaging temperature of electrolyte
$\overline{X}$	Axial coordinate in wave frame
x	Axial coordinate in dimensionless form
$\overline{E}_{\overline{X}}$	Axial electric field
$\overline{U}$	Axial velocity component in wave frame
u	Axial velocity component in dimensionless form
K_B	Boltzmann constant
Br	Brinkman number
D_B	Brownian diffusion coefficient
Nb	Brownian motion parameter
C_0, C_1	Concentration at walls
z	Charge balance
ρ_e	Density of net ionic energy
λ_d	Debye-length of electric double layer

$\in_1$	Dielectric constant
φ	Dimensionless potential distribution
$\bar{t}$	Time
α	Dimensionless fluid parameter
Nt	Dimensionless thermophoresis parameter
θ	Dimensionless temperature
ϕ	Dimensionless concentration
D_c	Diffusivity of chemical species
Ec	Eckert number
e	Electronic charge
σ_e	Electric conductivity
k	Electro-osmotic parameter
E_S	Entropy generation number
$S_{ij}, i, j = 1, 2, 3$	Extra stress tensor
ρ_f	Fluid density
Be	Bejan number
a_1, a_2	Half widths of the channel
S	Joule heating parameter
U_{hs}	Helmholtz-Smoluchowski velocity
T_m	Mean temperature of fluid
$\underline{C}$	Nanoparticle concentration
Nu	Nusselt's number
Pe	Peclet number
Φ	Phase difference
n	Power law index
$\overline{P}$	Pressure in wave frame
$\overline{V}$	Radial (transverse) velocity component in wave frame
v	Radial (transverse) velocity component in dimensionless form
Re	Reynolds number
C_f	Specific heat capacity of fluid
C_p	Specific heat capacity of nanoparticles
Sh	Sherwood number
$\underline{\psi}$	Steam function
$\overline{T}$	Temperature
T_0, T_1	Temperature at walls
D_T	Thermophoresis diffusion coefficient
K_f	Thermal conductivity
F	Flow rate in wave frame
y	Transverse coordinate in dimensionless form
$\overline{Y}$	Transverse coordinate in wave frame
δ	Wave number
H_1, H_2	Lower and upper walls
h_1, h_2	Lower and upper walls in dimensionless form
We	Weissenberg number
ξ_1, ξ_2	Zeta potentials at walls
R_ξ	Zeta potential ratio parameter

1 Introduction

The peristaltic transport phenomenon is commonly observed in different biological systems and mechanical processes. The peristaltic phenomenon is associated to the relaxation and contraction of a tabular structure. In the peristaltic process, the bio-fluids or physiological liquids move with applications of sinusoidal waves. Various applications of this flow pattern are observed in the biomedical sciences and human body. Yasmin and Iqbal [1] presented the peristaltic pattern due to ionic liquid in the porous channel with additional thermos-diffusion effects. Iqbal et al. [2] reported the Maxwell fluid associated to the peristaltic phenomenon. Nisar and Yasmin [3] analyzed the peristaltically driven flow of the Carreau–Yasuda model with bioconvective applications. The Casson fluid with peristaltic applications was observed by Yasmin and Nisar [4]. During the recent few years, electroosmotic flow, which is a suitable mechanism for transporting biological fluids in small ducts and capillaries electroosmotic flow occurs due to the application of a strong electric field that acts on the electric charges present in the electric double layer (EDL) at the boundaries of the conduit. Electroosmotic flow has many applications in fabrication, mixing of fluid in microfluidic devices, and pumping, as reported by Lin et al. [5] and Kim et al. [6]. Electroosmotic flow has many applications in bioengineering, such as sperm plasma separation and fluorescence-activated cell sorting mechanisms described by Jiang et al. [7] and Yao et al. [8]. Misra et al. [9] applied Debye-Hückel linearization to report the influence of an external electric field on the transport of micro-polar fluid through a vibrating micro-channel. The combined effects of electro-kinetics and peristalsis on the transport of a fluid in a conduit are reported by Chakraborty [10] for the first time. In their study, Tripathi et al. [11] investigated how electroosmosis affected the peristaltic flow of sperm in a micro-vessel. The effects of electroosmosis on the peristaltic transport of a rheological model characterized by coupled stress in a complex wavy channel are studied by Tripathi et al. [12]. The green function approach is used to solve the governing differential equation to discuss the endoscopic effects on the electroosmotic flow by Moghadam et al. [13]. Javid et al. [14] used biological assumptions based on the creeping assessment and Debye-Hückel approach while identifying the special effects of electroosmosis on the cilia-assisted flow in a non-uniform channel. Different zeta potentials were used by Abbasi et al. [15] to study the peristaltic movement of an Oldroyd 4-constant fluid in a channel that was not flat. Narla et al. [16] used the long wavelength and creeping transport assumptions to discuss the mutual impacts of electroosmosis and sinusoidal motion in a curved channel. Zeeshan et al. [17] and Asghar et al. [18] focused on deducing the influence of both electric and magnetic fields on the channel flow of coupled stress fluid. They analyzed the electro-osmotic flow in a complex wavy-inclined channel. The sound influences of Hartman number on the electroosmotic pumping of Jeffery fluid (viscoelastic fluid) in an asymmetric channel with different peristaltic flow features are discussed by Magesh et al. [19]. Eytan et al. [20] used Newtonian liquid relations to access biomimetic propulsion in a tapered channel. They have used sperm as Newtonian fluid in their investigation under creeping postulates. Narla et al. [21] visualized a mathematical formulation to investigate the viscoelastic embryo transport in the uterus under the influence of both peristalsis and electroosmosis.

Another important field of research is going to increase among researchers in the past two decades related to nanofluid transportations due to their thermal features. The nanofluids are decomposition of metallic particles with some based liquid. High thermal performances are predicted for nanomaterials due to excellent thermos-physical properties. To enhance the thermal mechanisms and heat transfer phenomenon, the nanomaterials play a significant role. Even nanofluids are effective at low temperature due to peak thermal performances. At low temperature, the dynamic of boosted thermal conductivity may be less incentive; however, the nanomaterials can be still beneficiary. The significance of nanomaterials with low temperature rate can be observed in refrigeration for maintaining the optimal heat efficiency. Buongiorno [22] evaluated the special thermal convective transport of nanomaterials under the fluctuating features. Prakash et al. [23] used the lubrication approach to analyze the thermal conductivity of nanofluid in a channel under the influence of both electroosmosis and peristalsis. They presented the analysis for different features for the transport of nanofluid with assisted and opposing electric fields. The Buongiorno model is utilized by Tripathi et al. [24] to simulate the simultaneous effects of joule heating and buoyancy forces in electroosmotic modulated peristaltic transport through a complex wavy channel. Farooq et al. [25] analyzed the electroosmotic transport of hybrid nanofluid in a complex wavy channel with different zeta potentials at both walls. In this analysis, temperature-dependent properties of sperm as a base fluid are reported. Das and Barman [26] analyzed the simultaneous effects of Hall current and ionic slip in the electroosmotic modulated peristaltic transport of hybrid nanofluid in a channel with different wave frames. The theoretical results of this study are very effective in the design of electromagnetic pumps and solar collectors. Prakash et al. [27] performed a numerical simulation to analyze the heat transfer phenomena in a sperm flow altered by electroosmosis through a microchannel. Ramesh and Prakash [28] talked about a thermal analysis of peristaltic transport in a vessel with Sutterby material supported by tiny particles. The study took place when there were both slip features and electroosmotic pumping. In this theoretical analysis, the graphical results for thermal characteristics are compared in view of negative numerical values and positive values of the joule heating parameter. Simultaneous effects of thermal radiation and joule heating on the transport of generalized Newtonian nanofluid characterized by Prandtl Eyring in a tapered channel via peristalsis and electroosmotic are reported by Abbasi et al. [29]. Zeeshan et al. [17] exclusively reported mathematical modeling and analysis to study the impact of different zeta potentials and heat sources on the electroosmotic modulated pumping of nanofluid through a complex wavy rectangular duct. Prakash et al. [30] carried out a theoretical study to report the applications of smart pumping in various energy systems by analyzing the peristaltic flow of pseudoplastic nanofluid in a channel via electroosmosis. Akram et al. [31] talked about how a methanol-based Sisko nanofluid moved peristaltically through a narrow channel while being affected by both electroosmosis and a porous medium at the same time. It is noticed that both the velocity and temperature of nanofluid are strongly dependent on the mechanism of electroosmosis. In another attempt, Akram et al. [32] analyzed the electroosmotic modulated peristaltic flow of nanofluid with nanoparticles through a curved channel. The graphical results verify that electroosmosis is effective in several features of transport and convective heat transfer.

Entropy generation (EG) has a vital role in regulating energy losses in the power-generating mechanism and the disorganization of thermodynamic systems. According to the Second Law of Thermodynamics, entropy minimization factors are like kinetic energy, vibration, internal molecular fraction, and spinning movement. Bejan [33] discussed the use of EG in different flow configurations. Additionally, the geometrical parameters have a momentous impact on the EG characteristics. Biological flow assumptions like creeping transport and long wavelength are used to deliberate the EG through a channel in the presence of electrokinetic pumping by Ranjit and Shit [34]. Hayat et al. [35] deliberated EG applications in the peristaltic transport of viscoelastic under the Jeffery model in a porous medium. The theoretical effect of electrokinetic pumping and non-Darcy porous medium on sinusoidal motion is examined by Noreen and Ain [36]. Abbasi et al. [37] performed

EG outcomes and thermal clarification of the peristaltic pumping of nanofluid. Nawaz et al. [38] described the impact of Lorentz force on EG in a curved domain with slippery walls. The impacts of both thermal and velocity slips on EG and thermal characteristics in electroosmotic peristaltic transport of two-layered flow are examined by Ranjit et al. [39]. The simultaneous effects of convective heat transfer and Lorentz force on the irreversibility and EG due to the peristaltic transport of generalized Newtonian fluid in a channel are addressed by Bhatti et al. [40]. Mabood et al. [41] examine the influence of electroosmotic force on EG in the transport of Eyring-Powell fluid in a channel. Abbasi et al. [42] showed a better thermal model to study how electroosmosis affects the pumping of Sutterby nanofluid through a channel that gets narrower at one end. Akram et al. [43] examine the effects of electroosmosis on the peristaltic transport of Rabinowitsch nanofluid in a channel. Sujith et al. [44] computed EG numerically by employing the finite element method for electroosmotic flow in a microchannel under the influence of slip boundaries. Akbar and Alotaibi [45] develop a mathematical model to analyze EG and irreversibility effects in electroosmotic modulated peristaltic transport in the presence of thermal radiation and non-linear mixed convection. A mathematical model was made by Gul et al. [46] to study EG in the peristalsis of Carreau nanofluid in an inclined asymmetric channel. An abstract model is established by Guedri et al. [47]. They present the simultaneous effects of joule heating, electrokinetic pumping, and viscous dissipation on EG and irreversibility in a curved channel.

The aim of the current analysis is to inspect the peristaltic-driven flow of Carreau-Yasuda nanofluid due to the asymmetric channel. The flow pattern is subject to the electrical force. The significance of electroosmotic effects has been adopted. The observations for thermal phenomenon are associated to the Joule heating effects. The zeta potentials at both surfaces of the channel are implemented for asymmetric channel. The model is developed by utilizing the fundamental laws along with the Poisson-Boltzmann equation. The governing system is developed under the biological flow assumptions. The numerical solutions are obtained with the help of the shooting method for numerous flow features. The graphs are plotted in Mathematica. The interpretation of flow graphs with respect to the involved variables in the given flow problem is presented. The current model is structured as: Section 2 presents the formulation of the problem. Section 3 deals with solution methodology, while the discussion of results is presented in Section 4. The validation of results has been presented in Section 5. In Section 6, key findings are summarized while applications of the current model are incorporated in Section 7.

2 Formulation of Problem

Consider the 2D flow of Carreau-Yasuda nanofluid having constant volume in an asymmetric geometry. Let the net width of the geometry be $a_1 + a_2$ and wave speed is c. Cartesian coordinates are being followed in ways that $\overline{X}$ axes are reflected in flow direction while $\overline{Y} - axis$ is orthogonal to the flow geometry [48]. Mathematically

$$H_2\left(\overline{X},\overline{t}\right) = a_1 + e_1 \sin\left(\frac{\xi_1}{\lambda}\left(\overline{X} - c\overline{t}\right)\right) + e_2 \sin\left(\frac{\xi_2}{\lambda}\left(\overline{X} - c\overline{t}\right)\right), \tag{1}$$

$$H_1\left(\overline{X},\overline{t}\right) = -a_2 - e_3 \sin\left(\frac{\xi_1}{\lambda}\left(\overline{X} - c\overline{t}\right) + \Phi\right) - e_4 \sin\left(\frac{\xi_2}{\lambda}\left(\overline{X} - c\overline{t}\right) + \Phi\right), \tag{2}$$

In which $\xi_i (i = 1, 2)$ are the distinct peristaltic wave amplitude, $\overline{t}$ being time, and λ is wavelength.

2.1 Governing Equations

The flow equations related to 2D nanofluid motion in a micro-channel in the physical influence of two external forces, one is an axial electric field $\overline{E}_{\overline{X}}$ and 2nd is the Joule heating, are [15, 16, 18, 19]:

$$\frac{\partial \overline{U}}{\partial \overline{X}} + \frac{\partial \overline{V}}{\partial \overline{Y}} = 0, \tag{3}$$

$$\rho_f\left(\frac{\partial \overline{U}}{\partial \overline{t}} + \overline{U}\frac{\partial \overline{U}}{\partial \overline{X}} + \overline{V}\frac{\partial \overline{U}}{\partial \overline{Y}}\right) = -\frac{\partial \overline{P}}{\partial \overline{X}} + \frac{\partial \overline{S}_{\overline{XX}}}{\partial \overline{X}} + \frac{\partial \overline{S}_{\overline{XY}}}{\partial \overline{Y}} + \rho_e \overline{E}_{\overline{X}}, \tag{4}$$

$$\rho_f\left(\frac{\partial \overline{V}}{\partial \overline{t}} + \overline{U}\frac{\partial \overline{V}}{\partial \overline{X}} + \overline{V}\frac{\partial \overline{V}}{\partial \overline{Y}}\right) = -\frac{\partial \overline{P}}{\partial \overline{Y}} + \frac{\partial \overline{S}_{\overline{YX}}}{\partial \overline{X}} + \frac{\partial \overline{S}_{\overline{YY}}}{\partial \overline{Y}}, \tag{5}$$

in which $\overline{U}$ and, $\overline{V}$ are axial and tangential velocity components, respectively, $\overline{P}$ is pressure. ρ_e is electric charge density, ρ_f is the density of fluid, and S_{ij} are components of extra stress tensor and it satisfy the explicit form:

$$S = \mu(\gamma_1)A_1, \tag{6}$$

In which A_1 denotes first Rivlin-Ericksen tensor and $\mu(\gamma_1)$ is apparent viscosity defined by [49–52]:

$$\mu(\gamma_1) = \mu_\infty + (\mu_0 - \mu_\infty)\left(1 + (\Gamma\gamma_1)^\alpha\right)^{\frac{n-1}{\alpha}}, \tag{7}$$

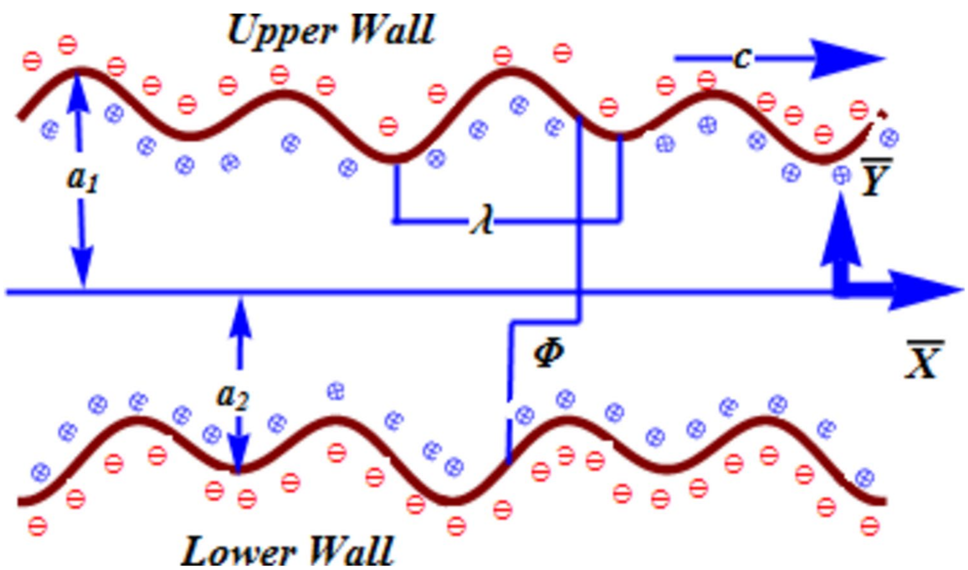

Fig. 1 Flow sketch

where

$$\gamma_1 = \sqrt{2tr\left(\frac{grad\boldsymbol{V} + grad\boldsymbol{V}^T}{2}\right)^2}, \tag{8}$$

In above equations μ_0 and μ_∞ are viscosities at zero and infinity, respectively, Γ and α are fluid parameters, respectively, n is the power law index, and $\boldsymbol{V}$ is the velocity of fluid.

The energy equation is defined as [53–59]:

$$\frac{\partial \overline{T}}{\partial \bar{t}} + \overline{U}\frac{\partial \overline{T}}{\partial \overline{X}} + \overline{V}\frac{\partial \overline{T}}{\partial \overline{Y}} = \left[\begin{array}{c} \frac{K}{(\rho C)_f}\left(\frac{\partial^2 \overline{T}}{\partial \overline{X}^2} + \frac{\partial^2 \overline{T}}{\partial \overline{Y}^2}\right) + \frac{\sigma_e}{(\rho C)_f}\overline{E}^2_{\overline{X}} \\ + \frac{(\rho C)_p}{(\rho C)_f}\left[D_B\left(\frac{\partial \overline{T}}{\partial \overline{X}}\frac{\partial \overline{C}}{\partial \overline{X}} + \frac{\partial \overline{T}}{\partial \overline{Y}}\frac{\partial \overline{C}}{\partial \overline{Y}}\right) + \frac{D_T}{T_m}\left(\left(\frac{\partial \overline{T}}{\partial \overline{X}}\right)^2 + \left(\frac{\partial \overline{T}}{\partial \overline{Y}}\right)^2\right)\right] \\ + \frac{1}{(\rho C)_f}\left(\overline{S}_{\overline{XX}}\frac{\partial \overline{U}}{\partial \overline{X}} + \overline{S}_{\overline{XY}}\left(\frac{\partial \overline{U}}{\partial \overline{Y}} + \frac{\partial \overline{V}}{\partial \overline{X}}\right) + \overline{S}_{\overline{YY}}\frac{\partial \overline{V}}{\partial \overline{Y}}\right) \end{array}\right], \tag{9}$$

The concentration of nanoparticles can be expressed by

$$\frac{\partial \overline{C}}{\partial \bar{t}} + \overline{U}\frac{\partial \overline{C}}{\partial \overline{X}} + \overline{V}\frac{\partial \overline{C}}{\partial \overline{Y}} = D_B\left(\frac{\partial^2 \overline{C}}{\partial \overline{X}^2} + \frac{\partial^2 \overline{C}}{\partial \overline{Y}^2}\right) + \frac{D_T}{T_m}\left(\frac{\partial^2 \overline{T}}{\partial \overline{X}^2} + \frac{\partial^2 \overline{T}}{\partial \overline{Y}^2}\right), \tag{10}$$

In the above equations, σ_e is electric conductivity, K is thermal conductivity, ρ_p is the density of nanoparticles, (C_f, C_p) being base liquid heating capacitance and nanomaterials, D_B is Brownian motion, D_T is for thermophoresis factor, and T_m is the mean temperature.

2.2 Boundary Conditions

As at both lower and upper walls of the channel the fluid is at rest, so axial velocity should be zero (Fig. 1). Let T_0 and C_0 be temperature and concentrations at the lower wall, and T_1 and C_1 be temperature and concentrations at the upper wall of the channel, then the appropriate boundary conditions are:

$$\begin{array}{l} \overline{U} = 0, \overline{T} = T_0, \overline{C} = C_0 \ at \ \overline{Y} = H_1\left(\overline{X}, \bar{t}\right) \\ \overline{U} = 0, \overline{T} = T_1, \overline{C} = C_1 \ at \ \overline{Y} = H_2\left(\overline{X}, \bar{t}\right) \end{array}, \tag{11}$$

2.3 Electric Potential

The electric potential $\overline{\varphi}$, when a strong electric field is applied in the axial direction is described by

$$\frac{\partial^2 \overline{\varphi}}{\partial \overline{X}^2} + \frac{\partial^2 \overline{\varphi}}{\partial \overline{Y}^2} = -\frac{\rho_e}{\in_1}, \tag{12}$$

with $\in_1$ is dielectric constant and ρ_e is electrolyte electric density expressed by relation with electric charges by

$$\rho_e = -ez\left(\overline{\omega}_- - \overline{\omega}_+\right), \tag{13}$$

In which $\omega_\mp$ are negative and positive ions, e is the magnitude of electric charge, and z is charge balance. The potential distribution is expressed as

$$\begin{array}{l} \frac{\partial \overline{\omega}_\pm}{\partial \bar{t}} + \overline{U}\frac{\partial \overline{\omega}_\pm}{\partial \overline{X}} + \overline{V}\frac{\partial \overline{\omega}_\pm}{\partial \overline{Y}} = D_c\left(\frac{\partial^2 \overline{\omega}_\pm}{\partial \overline{X}^2} + \frac{\partial^2 \overline{\omega}_\pm}{\partial \overline{Y}^2}\right) \\ \pm \frac{ez}{k_B T\prime}\left(\frac{\partial}{\partial \overline{X}}\left(\omega_\pm \frac{\partial \overline{\varphi}}{\partial \overline{X}}\right) + \frac{\partial}{\partial \overline{Y}}\left(\omega_\pm \frac{\partial \overline{\varphi}}{\partial \overline{Y}}\right)\right). \end{array} \tag{14}$$

In which D_c, $T\prime$, and K_B stand for diffusivity of chemical species, the average temperature of electrolyte, and Boltzmann constant.

2.4 Linear Transformations

Introducing the following linear transformations [55–59]:

$$\left.\begin{aligned}\bar{x} = \bar{X} - c\bar{t}, y = \bar{Y}, \bar{u}(\bar{x},\bar{y}) = \bar{U}\left(\bar{X},\bar{Y},\bar{t}\right) - c, \bar{v}(\bar{x},\bar{y}) = \bar{V}\left(\bar{X},\bar{Y},\bar{t}\right), \bar{p}(\bar{x},\bar{y}) = \bar{P}\left(\bar{X},\bar{Y},\bar{t}\right),\\ \bar{T}(\bar{x},\bar{y}) = \bar{T}\left(\bar{X},\bar{Y},\bar{t}\right), \bar{C}(\bar{x},\bar{y}) = \bar{C}\left(\bar{X},\bar{Y},\bar{t}\right), \bar{\varphi}(\bar{x},\bar{y}) = \bar{\varphi}\left(\bar{X},\bar{Y},\bar{t}\right).\end{aligned}\right\} \tag{15}$$

Here, $\bar{x}$ is the vector form of the axial coordinate, $\bar{y}$ is vector form of the transverse coordinate, $\bar{u}$ is velocity illustration in the axial direction, $\bar{v}$ is transverse direction velocity component, $\bar{p}$ is vector form of the pressure, $\bar{T}$ is vector form of the temperature field, $\bar{C}$ is vector form of the mass concentration, and $\bar{\varphi}$ is the electro-osmotic function.

The governing equations along with electric field equations take the form

$$\frac{\partial\bar{u}}{\partial\bar{x}} + \frac{\partial\bar{v}}{\partial\bar{y}} = 0, \tag{16}$$

$$\rho_f\left(\bar{u}\frac{\partial\bar{u}}{\partial\bar{x}} + \bar{v}\frac{\partial\bar{u}}{\partial\bar{y}}\right) = -\frac{\partial\bar{p}}{\partial\bar{x}} + \frac{\partial\bar{S}_{\bar{x}\bar{x}}}{\partial\bar{x}} + \frac{\partial\bar{S}_{\bar{x}\bar{y}}}{\partial\bar{y}} + \rho_e\bar{E}_{\bar{x}}, \tag{17}$$

$$\rho_f\left(\bar{u}\frac{\partial\bar{v}}{\partial\bar{x}} + \bar{v}\frac{\partial\bar{v}}{\partial\bar{y}}\right) = -\frac{\partial p}{\partial\bar{y}} + \frac{\partial\bar{S}_{\bar{y}x}}{\partial\bar{x}} + \frac{\partial\bar{S}_{\bar{y}\bar{y}}}{\partial\bar{y}}, \tag{18}$$

$$\bar{u}\frac{\partial\bar{T}}{\partial\bar{x}} + \bar{v}\frac{\partial\bar{T}}{\partial\bar{y}} = \begin{aligned}&\frac{K_f}{(\rho C)_f}\left(\frac{\partial^2\bar{T}}{\partial\bar{x}^2} + \frac{\partial^2\bar{T}}{\partial\bar{y}^2}\right) + \frac{\sigma_e}{(\rho C)_f}\bar{E}^2{}_{\bar{x}}\\ &+\frac{(\rho C)_p}{(\rho C)_f}\left[D_B\left(\frac{\partial\bar{T}}{\partial\bar{x}}\frac{\partial\bar{C}}{\partial\bar{x}} + \frac{\partial\bar{T}}{\partial\bar{y}}\frac{\partial\bar{C}}{\partial\bar{y}}\right) + \frac{D_T}{T_m}\left(\left(\frac{\partial\bar{T}}{\partial\bar{x}}\right)^2 + \left(\frac{\partial\bar{T}}{\partial\bar{y}}\right)^2\right)\right],\\ &+\frac{1}{(\rho C)_f}\left(\bar{S}_{\bar{x}\bar{x}}\frac{\partial\bar{u}}{\partial\bar{x}} + \bar{S}_{\bar{x}\bar{y}}\left(\frac{\partial\bar{u}}{\partial\bar{y}} + \frac{\partial\bar{v}}{\partial\bar{x}}\right) + \bar{S}_{\bar{y}\bar{y}}\frac{\partial\bar{v}}{\partial\bar{y}}\right),\end{aligned} \tag{19}$$

$$\bar{u}\frac{\partial\bar{C}}{\partial\bar{x}} + \bar{v}\frac{\partial\bar{C}}{\partial\bar{y}} = D_B\left(\frac{\partial^2\bar{C}}{\partial\bar{x}^2} + \frac{\partial^2\bar{C}}{\partial\bar{y}^2}\right) + \frac{D_T}{T_m}\left(\frac{\partial^2\bar{T}}{\partial\bar{x}^2} + \frac{\partial^2\bar{T}}{\partial\bar{y}^2}\right), \tag{20}$$

$$\frac{\partial^2\bar{\varphi}}{\partial\bar{x}^2} + \frac{\partial^2\bar{\varphi}}{\partial\bar{y}^2} = -\frac{\rho_e}{\epsilon_1}, \tag{21}$$

$$\bar{u}\frac{\partial\bar{\omega}_\pm}{\partial\bar{x}} + \bar{v}\frac{\partial\bar{\omega}_\pm}{\partial\bar{y}} = D_c\left(\frac{\partial^2\bar{\omega}_\pm}{\partial\bar{x}^2} + \frac{\partial^2\bar{\omega}_\pm}{\partial\bar{y}^2}\right) \pm \frac{ez}{K_BT'}\left(\frac{\partial}{\partial\bar{x}}\left(\omega_\pm\frac{\partial\bar{\varphi}}{\partial\bar{x}}\right) + \frac{\partial}{\partial\bar{y}}\left(\omega_\pm\frac{\partial\bar{\varphi}}{\partial\bar{y}}\right)\right). \tag{22}$$

2.5 Dimensionless Formulations and Biological Assumptions

The dimensionless formulation is carried out by using the following dimensionless variables and stream function ψ defined in terms of velocity components are $u = \partial\psi/\partial y$ and $v = -\delta\partial\psi/\partial x$.

$$\begin{gathered}x = \frac{\bar{x}}{\lambda}, y = \frac{\bar{y}}{a_1}, u = \frac{\bar{u}}{c}, v = \frac{\bar{v}}{c}, \theta = \frac{\bar{T}-T_0}{T_1-T_0}, \phi = \frac{\bar{C}-C_0}{C_1-C_0}, p = \frac{a_1^2\bar{p}}{c\lambda\mu_f},\\ S_{ij} = \frac{c\mu_f}{a_1}S_{\bar{ij}}, \delta = \frac{a_1}{\lambda}, Re = \frac{ca_1\rho_f}{\mu_f}, \varphi = \frac{ez}{K_BT\prime}\bar{\varphi}, \omega = \frac{\bar{\omega}}{\omega_0}, U_{hs} = \frac{E_\xi\epsilon_1K_BT\prime}{ezc\mu_f},\\ Pr = \frac{\mu_f(C_p)_f}{K_f}, S = \frac{\sigma_eE_x^2a_1^2}{K_f(T_1-T_0)}, h_1 = \frac{H_1}{a_1}, h_2 = \frac{H_2}{a_1}, B_j = \frac{e_j}{a_1}, d = \frac{a_2}{a_1},\\ Ec = \frac{c^2}{C_p(T_1-T_0)}, Nb = \frac{(\rho c)_pD_B(C_1-C_0)}{(\rho c)_f\nu_f}, Nt = \frac{(\rho c)_pD_T(T_1-T_0)}{(\rho c)_f\nu_f},\\ Sc = \frac{\nu_f}{D_B}, Pe = ReSc, Br = PrEc, We = \frac{\Gamma c}{a_1}\end{gathered} \tag{23}$$

After using the above dimensionless variables, the governing equations after using the following biological assumptions take the form.

- Long wavelength
- Creeping transport
- Debye-Hückel linearization

$$\frac{\partial p}{\partial x} = \frac{\partial S_{xy}}{\partial y} + k^2U_{hs}\varphi, \tag{24}$$

$$\frac{\partial p}{\partial y} = 0, \tag{25}$$

$$\frac{\partial^2\theta}{\partial y^2} + Br\frac{\partial^2\psi}{\partial y^2}S_{xy} + \Pr\left(Nb\frac{\partial\theta}{\partial y}\frac{\partial\phi}{\partial y} + Nt\left(\frac{\partial\theta}{\partial y}\right)^2 + S\right) = 0, \tag{26}$$

$$\frac{\partial^2\phi}{\partial y^2} + \frac{Nt}{Nb}\frac{\partial^2\theta}{\partial y^2} = 0, \tag{27}$$

$$\frac{\partial^2\Phi}{\partial y^2} = -k^2\left(\frac{\omega_+ - \omega_-}{2}\right), \tag{28}$$

$$\frac{\partial^2\omega_\pm}{\partial y^2} \pm \frac{\partial}{\partial y}\left(\omega_\pm\frac{\partial\varphi}{\partial y}\right) = 0, \tag{29}$$

In which U_{hs} is the electro-osmotic velocity, Br is the Brinkman number, Pr is the Prandtl number, Nb is the dimensionless Brownian motion parameter, Nt is the thermophoresis parameter, and S is joule heating parameter. The boundary constraints are:

$$\left.\begin{array}{l}\omega_{\pm} = 1 \; at \; \varphi = 0, \\ \frac{\partial \omega_{\pm}}{\partial y} = 0 \; at \; \frac{\partial \varphi}{\partial y} = 0.\end{array}\right\} \tag{30}$$

Taking

$$\omega_{\pm} = Exp(\mp\varphi), \tag{31}$$

$$\frac{\partial^2 \varphi}{\partial y^2} = k^2 sin\, h(\varphi), \tag{32}$$

where $k = a_1 ez\sqrt{\frac{2n_0}{\in_1 K_B T\prime}} = a_1/\lambda_d$ is the electro-osmotic parameter. Implementing the Debye – Huckel technique $sinh(\varphi) \cong \varphi$, Eq. (21) is written as:

$$\frac{\partial^2 \varphi}{\partial y^2} = k^2 \varphi. \tag{33}$$

In view of constraints $= \xi_1 \varphi = \xi_2$, the potential function is:

$$\varphi(y) = \xi_1 \frac{\sinh\left[k\left(y - h_2\right)\right] - R_{\xi}\sinh\left[k\left(y - h_1\right)\right]}{\sinh\left[k\left(h_1 - h_2\right)\right]}, \tag{34}$$

in which $R_{\xi} = \xi_2/\xi_1$ is zeta potential to walls ratio and λ_d is the Debye-length of EDL.

Eliminating pressure from Eqs. (24) and (25), the governing equations take the form

$$\frac{\partial^2 S_{xy}}{\partial y^2} + k^2 U_{hs}\frac{\partial \varphi}{\partial y} = 0, \tag{35}$$

$$\frac{\partial^2 \theta}{\partial y^2} + Br\frac{\partial^2 \psi}{\partial y^2}S_{xy} + \Pr\left(Nb\frac{\partial \theta}{\partial y}\frac{\partial \phi}{\partial y} + Nt\left(\frac{\partial \theta}{\partial y}\right)^2 + S\right) = 0, \tag{36}$$

$$\frac{\partial^2 \phi}{\partial y^2} + \frac{Nt}{Nb}\frac{\partial^2 \theta}{\partial y^2} = 0, \tag{37}$$

After using dimensionless variables, the value of the shear stress component is

$$S_{xy} = \left(1 + \left(We\frac{\partial^2 \psi}{\partial y^2}\right)^{\alpha}\right)^{\frac{n-1}{\alpha}}.$$

In which We is the Weissenberg number, n is the power law index, and α is the fluid parameter. The boundary constraints are:

$$\begin{array}{l}\psi = -\frac{F}{2}, \frac{\partial \psi}{\partial y} = -1, \theta = 1, \phi = 1 \; at \; y = h_2, \\ \psi = \frac{F}{2}, \frac{\partial \psi}{\partial y} = -1, \theta = 0, \phi = 0 \; at \; y = h_1.\end{array} \tag{38}$$

In which F is the volumetric flow rate.

The mathematical expressions for the Nusselt number and Sherwood number are [26, 27]

$$Nu = \frac{\partial \theta}{\partial y}\frac{\partial h_2}{\partial x}, \tag{39}$$

$$Sh = \frac{\partial \phi}{\partial y}\frac{\partial h_2}{\partial x}, \tag{40}$$

2.6 Entropy Generation

The volumetric entropy may be written as [40–44]

$$\left.\begin{array}{l}E_G = \underbrace{\frac{K_f}{T_m^2}\left(\left(\frac{\partial \overline{T}}{\partial \overline{X}}\right)^2 + \left(\frac{\partial \overline{T}}{\partial \overline{Y}}\right)^2\right)}_{\text{thermal irreversibility}} + \underbrace{\frac{S_{\overline{X}\,\overline{X}}\frac{\partial \overline{U}}{\partial \overline{X}} + S_{\overline{X}\,\overline{Y}}\left(\frac{\partial \overline{U}}{\partial \overline{Y}} + \frac{\partial \overline{V}}{\partial \overline{X}}\right) + S_{\overline{Y}\,\overline{Y}}\frac{\partial \overline{V}}{\partial \overline{Y}}}{T_m}}_{\text{fluid fraction irreversibility}} \\ \underbrace{+\frac{RD}{C_m}\left(\left(\frac{\partial \overline{C}}{\partial \overline{X}}\right)^2 + \left(\frac{\partial \overline{C}}{\partial \overline{Y}}\right)^2\right) + \frac{RD}{T_m}\left(\frac{\partial \overline{C}}{\partial \overline{X}}\frac{\partial \overline{T}}{\partial \overline{X}} + \frac{\partial \overline{C}}{\partial \overline{Y}}\frac{\partial \overline{T}}{\partial \overline{Y}}\right)}_{\text{Diffusion irreversibility}} + \underbrace{\sigma_e E_{\overline{X}}^2}_{\text{joule heating}},\end{array}\right\} \tag{41}$$

Alternatively, the entropy generation number can be expressed as

$$E_S = \frac{E_G}{E_C} = E_G\frac{T_m^2 d_1^2}{K_f(T_1 - T_0)}, \tag{42}$$

After using scaling variables and creeping approximation, the entropy generation number is

$$E_S = \left(\frac{\partial \theta}{\partial y}\right)^2 + \frac{Br}{\chi}\left(\left(1 + \left(We\frac{\partial^2 \psi}{\partial y^2}\right)^{\alpha}\right)^{\frac{n-1}{\alpha}}\right) + \frac{\varpi}{\chi}\frac{\partial \theta}{\partial y}\frac{\partial \phi}{\partial y} + \frac{\varpi\omega}{\chi^2}\left(\frac{\partial \phi}{\partial y}\right)^2 + \frac{S}{\chi}, \tag{43}$$

In which $\chi = \frac{T_1 - T_0}{T_m}$, $\omega = \frac{C_1 - C_0}{C_m}$, and $\varpi = \frac{RD(C_1 - C_0)}{K_f}$.

The mathematical form of the Bejan number is

$$Be = \frac{\left(\frac{\partial \theta}{\partial y}\right)^2}{E_S}, \tag{44}$$

3 Solution Methodology

The system of ODEs (35–37) subject to boundary conditions (38) is non-linear. It is difficult to find a closed-form solution, so many computational techniques are reported by many researchers to compute such problems. The numerical

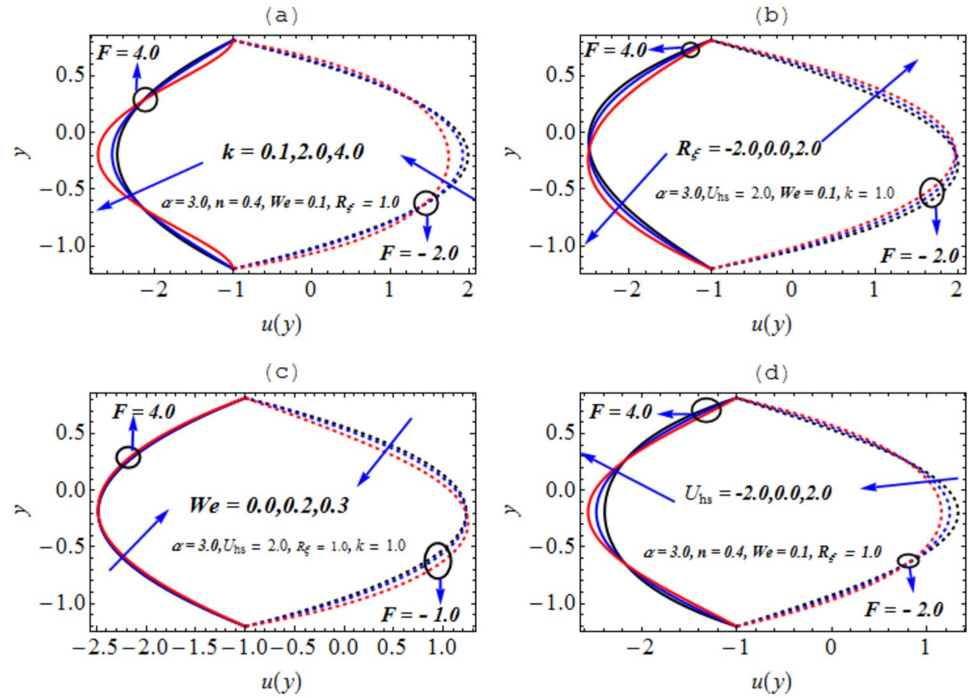

Fig. 2 Axial velocity against k, R_ξ, We, and U_{hs}

treatment is done for the system, and later, shooting computations are detected. The motivations for utilizing the shooting scheme are due to excellent accuracy. The shooting technique can effectively solve the complex flow problems with convincing accuracy. Moreover, this scheme does not involve any complicated discretization like other numerical tools. This technique reduces the order of the given flow problem into a single-order system. MATLAB software is used to compute the simulations. The solution procedure is followed with an accuracy of 10^{-6}.

4 Graphical Results and Discussion

The physical insight of parameters has been incorporated in view of different parameters. The formulated problem is based on some theoretical laws; therefore, all the parameters have assigned some fixed numerical values like $= 1.1, \Phi = \frac{\pi}{6}, F = -0.8, \alpha = 3.0, We = 0.1, U_{hs} = 2.0$, $Br = 1.0 = Pr$, $Nb = 0.2, Nt = 0.3$, and $n = 0.4$

4.1 Velocity Profile

Figure 2 is plotted to analyze the impact of the electroosmotic parameter (k), zeta potential ratio parameter (R_ξ), Weissenberg number (We), and electro-osmotic velocity (U_{hs}). The axial velocity $u(y)$ of sperm qualitatively shows different responses against electro-osmotic parameter k at numerous volumetric flow rates. For negative values of the flow rate $u(y)$ of sperm decreases at the channel heart while it grows near peristaltic walls. Electric force acts as an opposing force when U_{hs} is positive. By strengthening the electro-osmotic parameter, Debye-length of EDL decreases which restricts the transport at the heart and supports the transport near the wall. Furthermore, for positive values of flow rate, the magnitude of $u(y)$ behaves quite oppositely for k. Zeta potential ratio factor enhances $u(y)$ in the upper half (UH) while declining treatment is found in the lower regime in view of negative values associated to flow rate. Furthermore, the opposite response is noticed for positive values of zeta potential ratio parameter for increasing values of R_ξ, as it is a known fact that $R_\xi = \xi_2/\xi_1$ is the ratio between the zeta potentials at UH of the channel and LH of the channel. When R_ξ increases, the zeta potential of UH of the channel dominates the zeta potential of LH of the channel. As a result for the negative flow rate, the electric force assists the transport in UH of the channel. We raises the velocity in LH of the channel while restricts in LH of the channel for the negative flow rate. For the negative value of flow rate, the impact of We on $u(y)$ is dominant while for the positive value, this impact minimizes and opposite in behavior. As the electric field is changed from assisting to opposing, $u(y)$ of sperm decreases at the heart of the channel and rises in the vicinity of walls. This trend is followed by the negative value of F while the opposite trend in the main regime surface and near the walls for positive value of flow rate. These figures clearly disclosed that the velocity profiles are parabolic in nature.

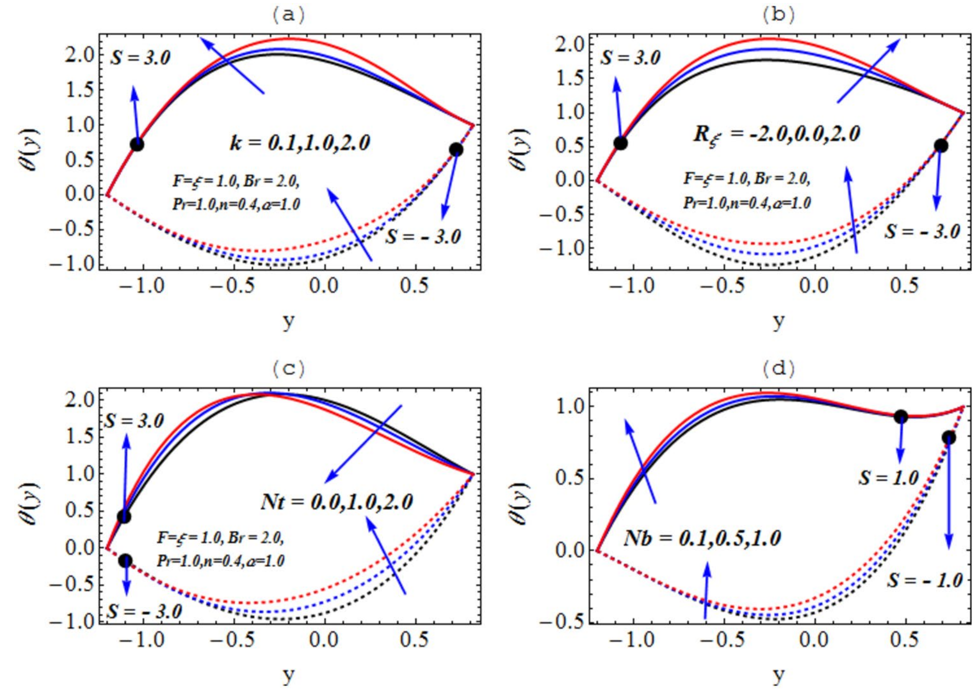

Fig. 3 Temperature profile against k, R_ξ, Nt, and Nb

4.2 Temperature Profile

The impact of electroosmotic parameter (k), zeta potential ratio parameter (R_ξ), thermophoresis diffusion parameter (Nt), Brownian motion parameter (Nb), Weissenberg number (We), and electro-osmotic velocity (U_{hs}) for $S = 3.0$ and $S = -3.0$ on the temperature of nanofluid is reported in Fig. 3. The temperature $\theta(y)$ of a sperm-based nanofluid is increasing function of electroosmotic parameter when $S = 3.0$ and decreasing function of electroosmotic parameter for the fixed value of other involved parameters. For $S = 3.0$, the impact of the electric field is opposing to the flow of sperm in a complex wavy tract, which restrict the movement of sperm in the tract. As a result, the internal kinetic energy of sperm rises, which enhances the temperature of the fluid at the heart of the channel and this response disappears near the boundaries. $\theta(y)$ of sperm-based

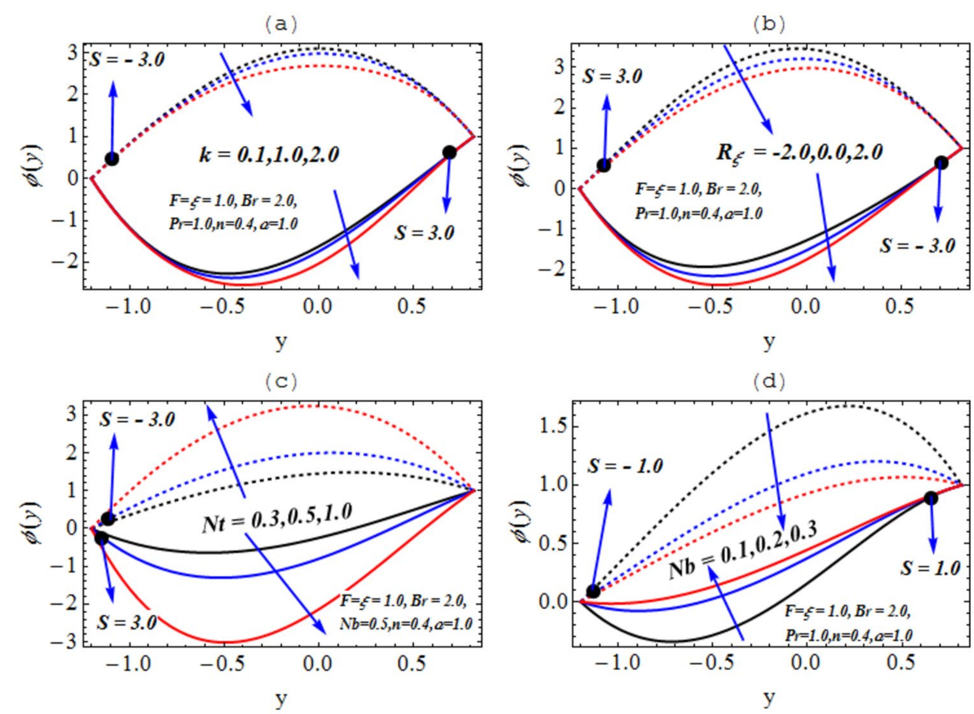

Fig. 4 Concentration profile against k, R_ξ, Nt, and Nb

nanofluid growths as zeta potential ratio parameter changed from negative to positive, i.e., $R_\xi = -2.0$ to $R_\xi = 2.0$ for opposing joule heating parameter $S = 3.0$ while this trend altered for assisting joule heating parameter. Thermophoresis diffusion rises the temperature of nanofluid for $S = 3.0$ in the LH of the channel while reverse actions are viewed in UH of the geometry. On the other hand, the declining trend is charted by temperature profile $\theta(y)$ for the enhancing thermophoresis diffusion in both halves of the channel for $S = -3.0$. Similarly, the rise in Brownian motion of nanoparticles in the sperm-based nanofluid rises $\theta(y)$ of sperm-based nanofluid for $S = 1.0$ while a decline is seen for $S = -1.0$.

4.3 Concentration Profile

The concentration profile of sperm-based nanofluid against electroosmotic parameter (k), zeta potential ratio parameter (R_ξ), thermophoresis diffusion parameter (Nt), Brownian motion parameter (Nb), Weissenberg number (We), and electro-osmotic velocity (U_{hs}) for $S = 3.0$ and $S = -3.0$ is depicted through Fig. 4. The concentration of nanoparticles in sperm-based nanofluid decreases against k for $S = -3.0$ and on the other hand, the rise in concentration is noticed against k for $S = 3.0$ through a complex wavy channel. The zeta potential ratio parameter decreases the concentration for $S = -3.0$ while on the other hand, zeta potential ratio parameter rises the concentration of nanoparticles in sperm-based nanoliquid for $S = 3.0$. The negative and positive values of Joule heating factor enrich the concentration impact. The Brownian motion parameter presents a decreasing trend in the concentration of nanoparticles for $S = 1.0$ as well as $S = -1.0$.

4.4 Streamlines

Figures 5 and 6 are plotted to analyze the impact of electroosmotic parameter k and zeta potential ratio R_ξ on streamline which depicts the trapping of bolus in the sperm flow through complex artery. The trapping phenomena are discussed for assisting electro kinetic pumping and opposing

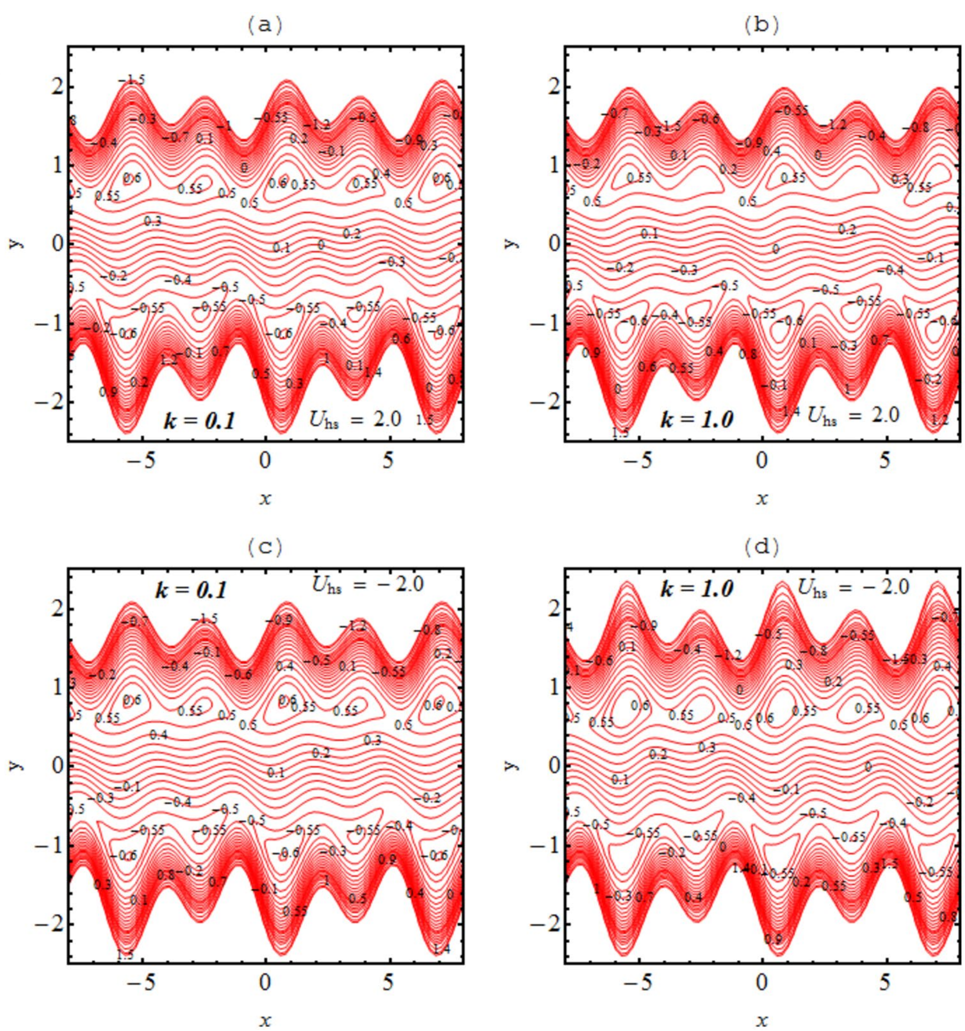

Fig. 5 Streamlines against k. Other parameters are $d = 1.1, \Phi = \frac{\pi}{6}, F = -0.8, \alpha = 3.0, We$ and $n = 0.4$

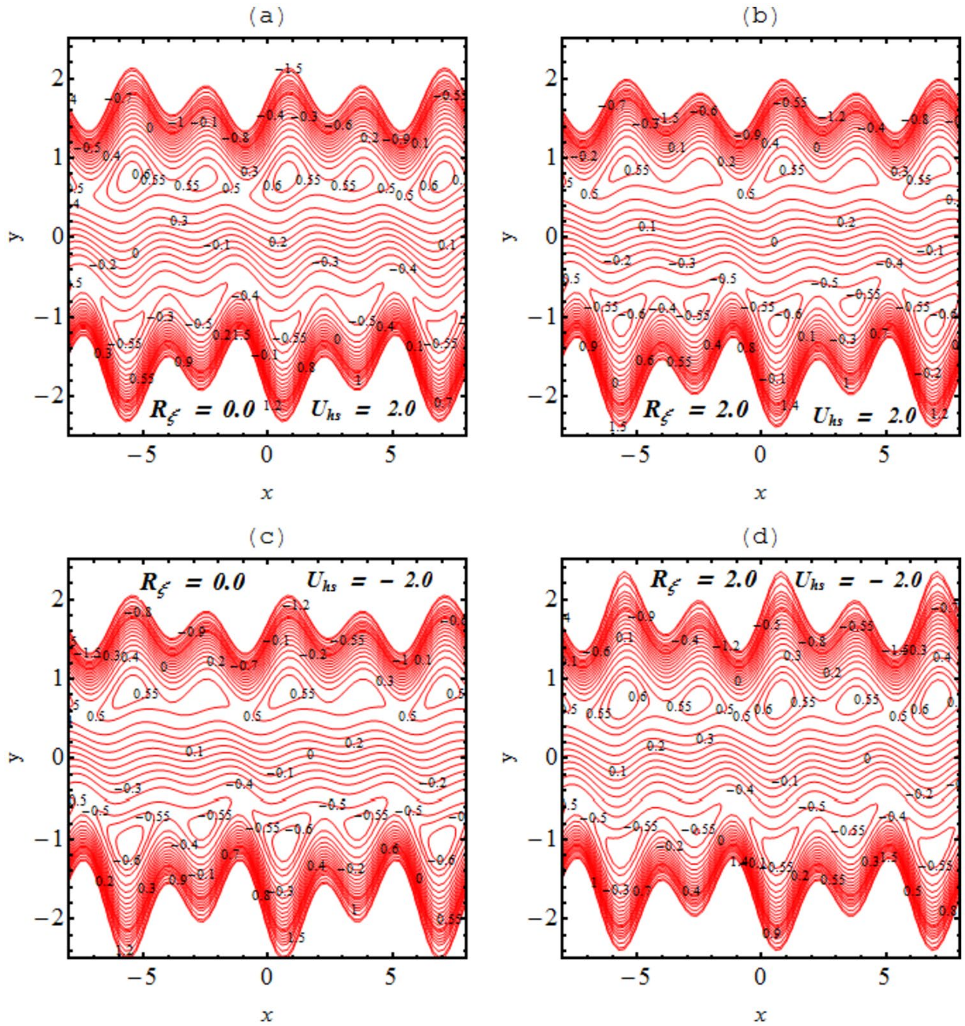

Fig. 6 Streamlines against R_ξ. Other parameters are $d = 1.1, \Phi = \frac{\pi}{6}, F = -0.8, \alpha = 3.0, We$ and $n = 0.4$

electro kinetic pumping. The rise in electroosmotic parameter causes the disappearance of bolus from UH against the reflecting electro kinetic pumping. Furthermore, the mass of trapping bolus rises in LH of the geometry with growth in electroosmotic force, as electroosmotic force acts in the conflicting trend of flow which is responsible for the trapping of nanofluid in LH of the channel. On the other hand, for assisting electro kinetic pumping, the fluid ruses in the UH of the channel under the influence of electroosmotic parameter. A similar response of streamlines against the zeta potential ratio parameter is noticed for seen for both assisting and opposing electro kinetic pumping.

4.5 Nusselt Number and Sherwood Number

In this subsection, the impact of electroosmotic parameter k, zeta potential ratio parameter R_ξ, Nt, and Nb on Nusselt factor and Sherwood number is presented and discussed by Figs. 7 and 8. The computational analysis and presentation are carried out for positive values and negative assigning values to joule heating constant. The rise in electroosmotic parameter reduces the Nusselt number for $S = 2.0$ while rises for $S = -2.0$. On the other hand, a similar response of Sherwood number is seen for the rising values of electroosmotic parameter k when $S = 2.0$ and $S = -2.0$. The zeta potential ratio parameter also decreases the heating phenomenon for $S = 2$ and enhances for $S = -2$. Furthermore, the thermophoresis parameter also reduces the heat transfer rate for $S = 2.0$ and $S = -2.0$. On the other hand, the mass transfer rate at the upper wall of the channel rises with increasing the thermophoresis diffusion parameter. A reduction in the Nusselt number is deduced for both cases of joule heating constant with leading Nb.

4.6 Entropy Generation

Entropy generation (EG) plays a significant role in the thermal optimization of various electro kinetic pumps. In this subsection, EG number is presented and discussed

Fig. 7 Nusselt number against k, R_ξ, Nt, and Nb

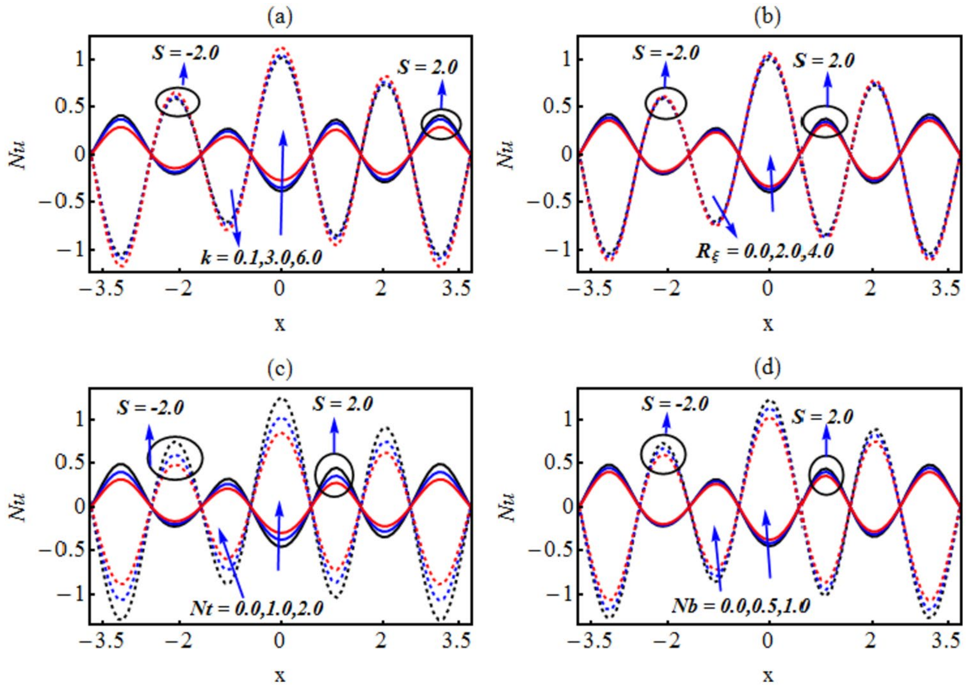

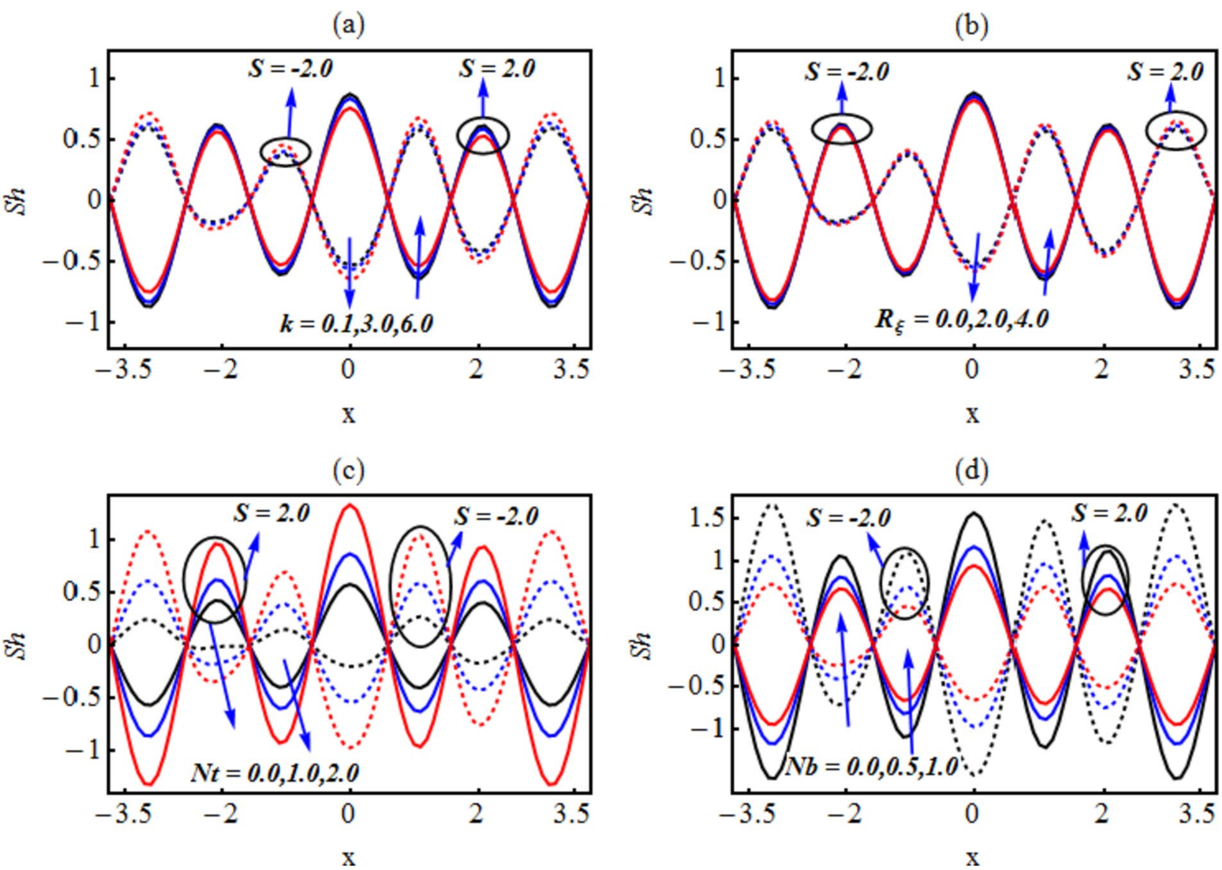

Fig. 8 Sherwood number against k, R_ξ, Nt, and Nb. Other parameters are $d = 1.1, \Phi = \frac{\pi}{6}, F = 1.0 = Br = Pr, \alpha = 3.0, We = 0.1, U_{hs} = 2.0$, and $n = 0.4$

for increasing values of electroosmotic parameter k, zeta potential ratio parameter R_ξ, thermophoresis parameter Nt, and Brownian diffusion parameter Nb. The impact of penetrating parameters for joule heating values is presented in Fig. 9. The electroosmotic parameter rises EG number for $S = 1.0$ as well as $S = -1.0$ in a complex wavy channel. As electroosmotic force is a drag force which restricts the transport, and as a result, the entropy of the system rises. Furthermore, EG number is bulky for $S = 1.0$ as compared to $S = -1.0$. EG number shows a decreasing trend against R_ξ. The thermophoresis parameter raises the EG number while the Brownian motion parameter reduces EG number for both positive and negative values of joule heating parameter.

4.7 Bejan Number

The variation of Bejan number against the rising values of electroosmotic parameter k, Brownian motion parameter Nb, zeta potential ratio parameter R_ξ, and thermophoresis parameter Nt is presented in Fig. 10. The irreversibility is analyzed and discussed for both assisting joule heating, i.e., $S = -1.0$, and opposing joule heating i.e. $S = 1.0$. The irreversibility is the increasing function of electroosmotic parameter while the decreasing function of zeta potential ratio parameter. On the other hand, thermophoresis diffusion reduces the Bejan number while Brownian diffusion coefficient rises the Bejan number.

5 Comparison of Obtained Results

For the substantiation of present results obtained in the present study, the comparison of the velocity profile is made with Noreen et al. [54]. The velocity profile for viscous fluid in the absence of electro kinetic pumping shows a good agreement (Fig. 11).

6 Key Findings

- Velocity decreases of the channel for $F = -2.0$ and increases at heart for $F = 4.0$ against the increasing values of k and U_{hs}.
- The temperature of nanofluid rises with electroosmotic parameter, zeta potential ratio parameter, and Brownian diffusion for positive case of joule heating.
- The concentration of nanoparticles grows with Nt while declines with Nb for both cases of joule heating parameter.
- Electroosmotic parameter fluid rushes in LH of the channel for opposing electro kinetic pumping while rushes in UH for assisting electro kinetic pumping.
- The number of trapping bolus reduces in UH of the channel against zeta potential ratio parameter for opposing electro kinetic pumping.
- Both Nusselt number and Sherwood number are decreasing function of Brownian motion parameter.

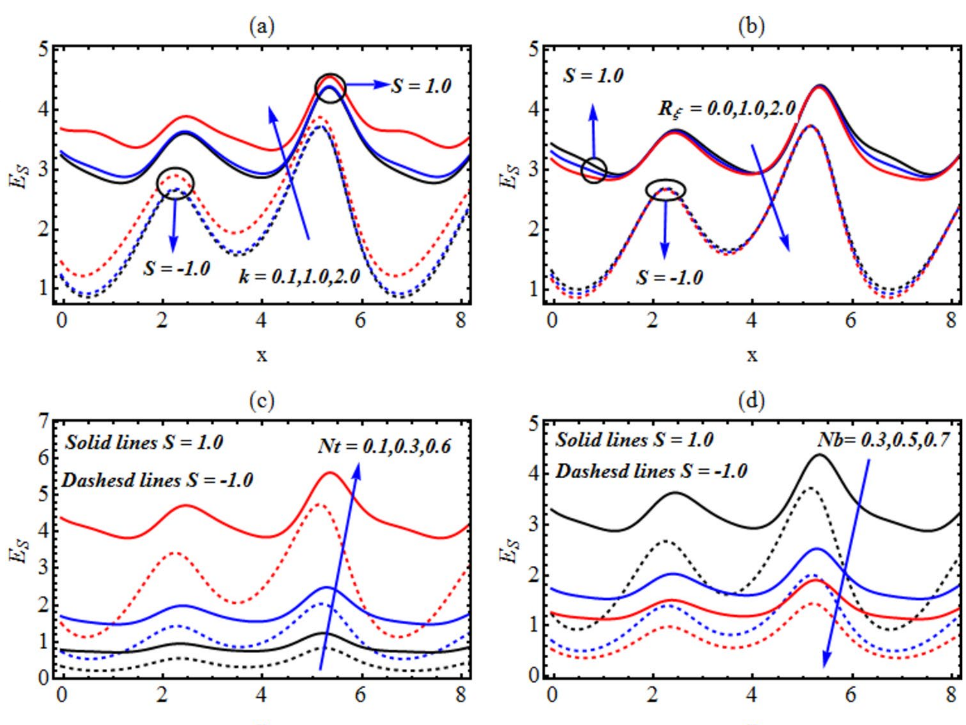

Fig. 9 Entropy generation number against k, R_ξ, Nt, and Nb. Other parameters are $d = 1.1, \Phi = \frac{\pi}{6}, F = -0.8, \alpha = 3.0, We$ $Br = 1.0 = Pr$, and $n = 0.4$

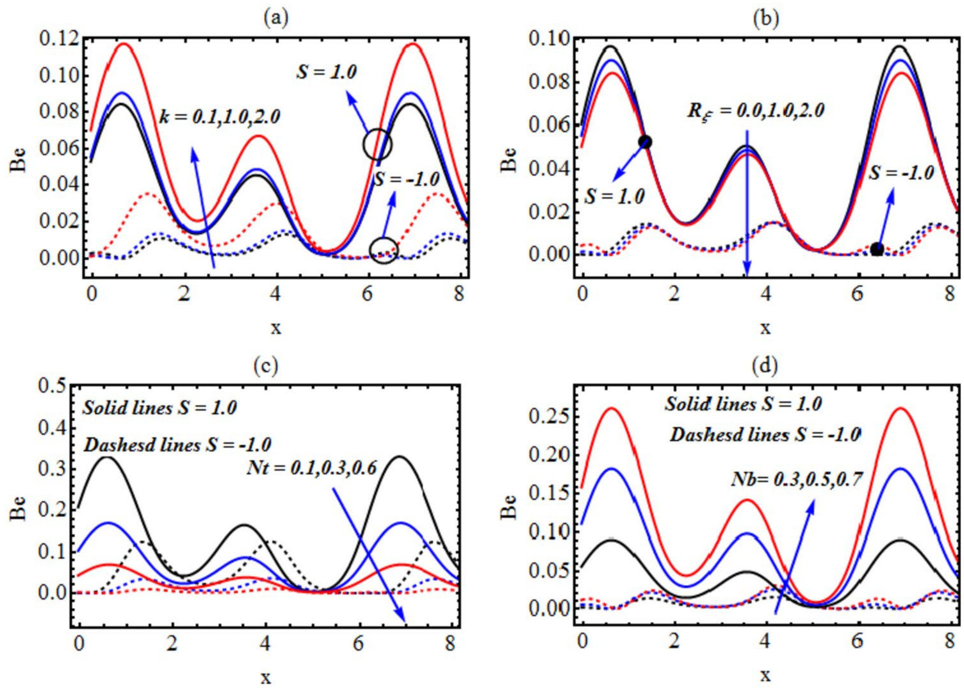

Fig. 10 Bejan number against k, R_ξ, Nt, and Nb. Other parameters are $d = 1.1, \Phi = \frac{\pi}{6}, F = -0.8, \alpha = 3.0, We$ $Br = 1.0 = Pr$, and $n = 0.4$

- The electroosmotic parameter and zeta potential ratio parameter reduce the heat transfer rate and mass transfer rate for $S = 2.0$.
- EG number shows an increasing trend against the rising values of electroosmotic parameter and thermophoresis diffusion.
- EG number shows a decreasing trend with the growth of zeta potential ratio parameter and Brownian diffusion.
- Bejan number is decreasing function of thermophoresis parameter while increasing function of Brownian motion parameter.
- Both EG number and Bejan number are large for $S = 1.0$ as compared to $S = -1.0$.

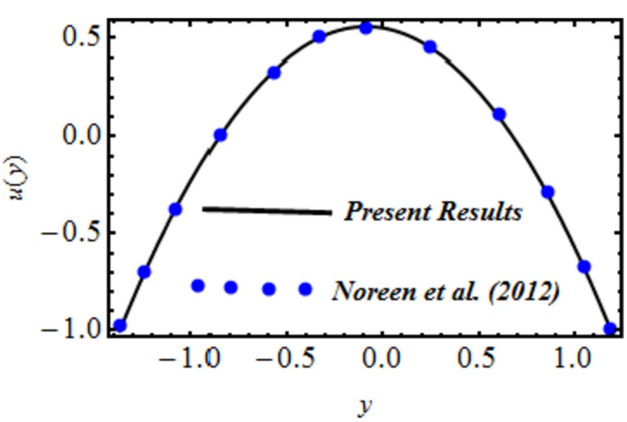

Fig. 11 Comparison of present results with Noreen et al. [54]

7 Applications of Current Model

This study has remarkable applications in industry and engineering sites, especially in the chemical domains. Here, we have observed the flow behavior of the Carreau fluid model; it gives us information regarding shear thinning and thickening of fluid nature which depends on suitable values of index parameter. Here, the outcomes of viscous liquid can easily be recovered by substituting $n = 1$, shear-thinning fluid is obtained by putting $n < 1$, and shear-thickening fluid is obtained by putting $n > 1$. This formulation further helps the researchers to understand the rheological pumping of nanofluid via divergent path or non-uniform domains/vessels under creeping theory. Additionally, this study tells the readers about the blood motion in a divergent vessel under the physical effects of the electric field. Normally, such types of motions are observed in the mechanical industry to manufacture the shape of peristaltic pumps or rollers which are based on creeping theory. These pumps are used in different chemical industries and engineering domains to reduce the human effect in better ways. Such types of studies can also be enhanced by using different nanoparticles that are productive in thermal enhancement. By using numerous rheological geometries, this study can also be elaborated. Furthermore, the special environment of sinusoidal waves is used in the present examination to boost the thermo-physical characteristics of nanoliquids under biological considerations.

Author Contribution A. Abbasi and W. Farooq provided the concept and edited the draft of the manuscript. Sami Ullah Khan and Adnan conducted the literature review and wrote the first draft of the manuscript. Arshad Riaz and M. M. Bhatti edited the final draft of the manuscript. The authors declare that all data were generated in-house and that no paper mill was used.

Data Availability The data that support the findings of this study are available from the corresponding author upon reasonable request.

Declarations

Ethics Approval Not applicable.

Conflict of Interest The authors declare that they have no conflict of interest.

References

1. H. Yasmin, N. Iqbal, Convective mass/heat analysis of an electroosmotic peristaltic flow of ionic liquid in a symmetric porous microchannel with soret and dufour. Math. Probl. Eng. **2021**, 1–14 (2021)
2. N. Iqbal, H. Yasmin, A. Bibi, A.A. Attiya, Peristaltic motion of Maxwell fluid subject to convective heat and mass conditions. Ain Shams Engineering Journal **12**(3), 3121–3131 (2021)
3. Z. Nisar, H. Yasmin, Analysis of motile gyrotactic micro-organisms for the bioconvection peristaltic flow of Carreau-Yasuda bionanomaterials. Coatings **13**(2), 314 (2023)
4. H. Yasmin, Z. Nisar, Mathematical analysis of mixed convective peristaltic flow for chemically reactive Casson nanofluid. Mathematics **11**(12), 2673 (2023)
5. C.-H. Lin, L.-M. Fu, Y.-S. Chien, Microfluidic T-form mixer utilizing switching electroosmotic flow. Anal. Chem. **76**, 5265 (2004)
6. B.J. Kim, S.Y. Yoon, K.H. Lee, H.J. Sung, Development of a microfluidic device for simultaneous mixing and pumping. Exp. Fluids **46**, 85 (2009)
7. H. Jiang, X. Weng, C.H. Chon, X. Wu, D. Li, A microfluidic chip for blood plasma separation using electro-osmotic flow control. J. Micromech. Microeng. **21**(8), 085019 (2011)
8. B. Yao, G.-A. Luo, X. Feng, W. Wang, L.-X. Chen, Y.-M. Wang, A microfluidic device based on gravity and electric force driving for flow cytometry and fluorescence activated cell sorting. Lab Chip **4**, 603 (2004)
9. J.C. Misra, S. Chandra, G.C. Shit, P.K. Kundu, Electroosmotic oscillatory flow of micropolar fluid in microchannels: application to dynamics of sperm flow in microfluidic devices. Appl. Math. Mech.-Engl. Ed. **35**, 749–766 (2014)
10. S. Chakraborty, Augmentation of peristaltic microflows through electro-osmotic mechanisms. J. Phys. D Appl. Phys. **39**, 5356 (2006)
11. D. Tripathi, A. Borode, R. Jhorar, O.A. Bég, A.K. Tiwari, Computer modelling of electro-osmotically augmented three-layered microvascular peristaltic sperm flow. Microvasc. Res. **114**, 65 (2017)
12. D. Tripathi, R. Jhorar, O. Anwar Bég, A. Kadir, Electro-magneto-hydrodynamic peristaltic pumping of couple stress biofluids through a complex wavy micro-channel. J. Mol. Liq. **236**, 358 (2017)
13. J. Moghadam, Electrokinetic-driven flow and heat transfer of a non-newtonian fluid in a circular microchannel. J. Heat Transfer **135**, 021705 (2013)
14. K. Javid, M. Riaz, Y.M. Chu, M. Ijaz Khan, S. Ullah Khan, S. Kadry, Peristaltic activity for electro-kinetic complex driven cilia transportation through a non-uniform channel. Comput. Methods Programs Biomed. **200**, 926 (2021)
15. A. Abbasi, A. Zaman, W. Farooq, M.F. Nadeem, Electro-osmosis modulated peristaltic flow of oldroyd 4-constant fluid in a non-uniform channel. Indian J. Phys. Proc. Indian Assoc. Cultiv. Sci. **96**, 825 (2022)
16. V.K. Narla, D. Tripathi, O.A. Bég, Electro-osmotic nanofluid flow in a curved microchannel. Chin. J. Phys. **67**, 544 (2020)
17. A. Zeeshan, A. Riaz, F. Alzahrani, Electroosmosis-modulated bio-flow of nanofluid through a rectangular peristaltic pump induced by complex traveling wave with zeta potential and heat source. Electrophoresis. **42**, 2143 (2021)
18. Z. Asghar, M.W. Saeed Khan, M.A. Gondal, A. Ghaffari, Channel flow of non-Newtonian fluid due to peristalsis under external electric and magnetic field. Proc. Inst. Mech. Eng. Part E J. Process Mech. Eng. **236**, 2670 (2022)
19. A. Magesh, M. Kothandapani, V. Pushparaj, Electro-osmatic flow of Jeffrey fluid in an asymmetric micro-channel under the effect of magnetic field. J. Phys. Conf. Ser. **1850**, 012102 (2021)
20. O. Eytan, A.J. Jaffa, D. Elad, Peristaltic flow in a tapered channel: application to embryo transport within the uterine cavity. Med. Eng. Phys. **23**, 473 (2001)
21. V.K. Narla, D. Tripathi, O. Anwar Bég, Electro-osmosis modulated viscoelastic embryo transport in uterine hydrodynamics: mathematical modeling. J. Biomech. Eng. **141**, 021003 (2019)
22. J. Buongiorno, Convective transport in nanofluids. J. Heat Transfer **128**, 240 (2006)
23. J. Prakash, A. Sharma, D. Tripathi, Thermal radiation effects on electroosmosis modulated peristaltic transport of ionic nanoliquids in biomicrofluidics channel. J. Mol. Liq. **249**, 843 (2018)
24. D. Tripathi, A. Sharma, O. Anwar Bég, Joule heating and buoyancy effects in electro-osmotic peristaltic transport of aqueous nanofluids through a microchannel with complex wave propagation. Adv. Powder Technol. **29**, 639 (2018)
25. W. Farooq, A. Abbasi, K. Al-Khaled, S. U. Khan, Electro-osmosis optimized peristaltic flow of hybrid nanofluid in complex wavy channel with different zeta potentials and variable thermal properties. Wav. Random. Complex. Media. 1–23 (2022). https://doi.org/10.1080/17455030.2022.2108158
26. S. Das, B. Barman, Ramification of Hall and ion-slip currents on electro-osmosis of ionic hybrid nanofluid in a peristaltic microchannel. Bionanosci. **12**, 957 (2022)
27. J. Prakash, K. Ramesh, D. Tripathi, R. Kumar, Numerical simulation of heat transfer in sperm flow altered by electroosmosis through tapered micro-vessels. Microvasc. Res. **118**, 162 (2018)
28. K. Ramesh, J. Prakash, Thermal analysis for heat transfer enhancement in electroosmosis-modulated peristaltic transport of Sutterby nanofluids in a microfluidic vessel. J. Therm. Anal. Calorim. **138**, 1311 (2019)
29. A. Abbasi, F. Mabood, W. Farooq, S.U. Khan, Radiation and joule heating effects on electroosmosis-modulated peristaltic flow of Prandtl nanofluid via tapered channel. Int. Commun. Heat Mass Transf. **123**, 5183 (2021)
30. J. Prakash, M.G. Reddy, D. Tripathi, A.K. Tiwari, A model for electro-osmotic flow of pseudoplastic nanofluids in presence of peristaltic pumping: an application to smart pumping in energy systems, in *Nanotechnology for Energy and Environmental Engineering*. (Springer International Publishing, Cham, 2020), pp.185–213
31. J. Akram, N. S. Akbar, D. Tripathi, Numerical study of the electroosmotic flow of Al2O3–CH3OH Sisko nanofluid through a tapered microchannel in a porous environment. Appl. Nanosci. **10**, 4161–4176 (2020)
32. J. Akram, N.S. Akbar, M. Alansari, D. Tripathi, Electroosmotically modulated peristaltic propulsion of TiO2/10W40 nanofluid in curved microchannel. Int. Commun. Heat Mass Transf. **136**, 106208 (2022)

33. A. Bejan, A study of entropy generation in fundamental convective heat transfer. J. Heat Transfer **101**, 718 (1979)
34. N.K. Ranjit, G.C. Shit, Entropy generation on electro-osmotic flow pumping by a uniform peristaltic wave under magnetic environment. Energy (Oxf.) **128**, 649 (2017)
35. T. Hayat, S. Farooq, B. Ahmad, A. Alsaedi, Effectiveness of entropy generation and energy transfer on peristaltic flow of Jeffrey material with Darcy resistance. Int. J. Heat Mass Transf. **106**, 244 (2017)
36. S. Noreen, Q.U. Ain, Entropy generation analysis on electroosmotic flow in non-Darcy porous medium via peristaltic pumping. J. Therm. Anal. Calorim. **137**, 1991 (2019)
37. F.M. Abbasi, I. Shanakhat, S.A. Shehzad, Entropy generation analysis for peristalsis of nanofluid with temperature dependent viscosity and Hall effects. J. Magn. Magn. Mater. **474**, 434 (2019)
38. S. Nawaz, T. Hayat, A. Alsaedi, Numerical study for peristalsis of Siskonanomaterials with entropy generation. J. Therm. Anal. Calorim. **139**, 2129 (2020)
39. N.K. Ranjit, G.C. Shit, D. Tripathi, Entropy generation and Joule heating of two layered electroosmotic flow in the peristaltically induced micro-channel. Int. J. Mech. Sci. **153–154**, 430 (2019)
40. M.M. Bhatti, A. Riaz, L. Zhang, S.M. Sait, R. Ellahi, Biologically inspired thermal transport on the rheology of Williamson hydromagnetic nanofluid flow with convection: an entropy analysis. J. Therm. Anal. Calorim. **144**, 2187 (2021)
41. F. Mabood, W. Farooq, A. Abbasi, Entropy generation analysis in the electro-osmosis-modulated peristaltic flow of Eyring-Powell fluid. J. Therm. Anal. Calorim. **147**, 3815 (2022)
42. A. Abbasi, W. Farooq, S. U. Khan, H. Amer, M. I. Khan, Electroosmosis optimized thermal model for peristaltic flow of with Sutterby nanoparticles in asymmetric trapped channel. Eur. Phys. J. Plus **136**(12), 1207 (2021)
43. J. Akram, N.S. Akbar, D. Tripathi, Entropy generation in electroosmotically aided peristaltic pumping of MoS2 Rabinowitsch nanofluid. Fluid Dyn. Res. **54**, 015507 (2022)
44. T. Sujith, S.K. Mehta, S. Pati, Effect of finite size of ions on entropy generation characteristics for electroosmotic flow through microchannel considering interfacial slip. J. Therm. Anal. Calorim. **148**, 489 (2023)
45. Y. Akbar, H. Alotaibi, Electroosmosis-optimized thermal model for peristaltic transportation of thermally radiative magnetized liquid with nonlinear convection. Entropy (Basel) **24**, 530 (2022)
46. M. Gul, F.M. Abbasi, S.A. Shehzad, A. Shafee, Entropy generation for peristaltic motion of Carreau's fluid with mixture of ethylene glycol and boron-nitride nanoparticles. Phys. Scr. **95**, 035212 (2020)
47. K. Guedri, M. M. Lashin, A. Abbasi, S. U. Khan, W. Farooq, M. I. Khan, A. M. Galal, Biomedical and engineering aspects of nonlinear radiative peristaltic transport in chemically reactive sperm flow of Ellis nanofluid in an asymmetric channel with activation energy. Chin. J. Phys. (2022)
48. T. Hayat, B. Ahmed, F.M. Abbasi, A. Alsaedi, Numerical investigation for peristaltic flow of Carreau-Yasuda magneto-nanofluid with modified Darcy and radiation. J. Therm. Anal. Calorim. **137**, 1359–1367 (2019)
49. T. Hayat, R. Iqbal, A. Tanveer, A. Alsaedi, Mixed convective peristaltic transport of Carreau-Yasuda nanofluid in a tapered asymmetric channel. J. Mol. Liq. **223**, 1100 (2016)
50. S. Ayub, H. Zahir, A. Tanveer, Mixed convection and non-linear thermal radiative analysis for Carreau-Yasuda nanofluid in an endoscope. Int. Commun. Heat Mass Transf. **138**, 106371 (2022)
51. S.M. Kayani, S. Hina, M. Mustafa, A new model and analysis for peristalsis of Carreau-Yasuda (CY) nanofluid subject to wall properties. Arab. J. Sci. Eng. **45**, 5179 (2020)
52. G. Sucharitha, P. Lakshminarayana, N. Sandeep, Joule heating and wall flexibility effects on the peristaltic flow of magnetohydrodynamic nanofluid. Int. J. Mech. Sci. **131–132**, 52 (2017)
53. F.M. Abbasi, T. Hayat, B. Ahmad, Numerical analysis for peristalsis of Carreau-Yasuda nanofluid in an asymmetric channel with slip and Joule heating effects. J. Eng. Thermophys. **25**, 548 (2016)
54. S. Noreen, A. Alsaedi, T. Hayat, Peristaltic flow of pseudoplastic fluid in an asymmetric channel. J. Appl. Mech. **79**, 054501 (2012)
55. K. Javid, N. Ali, Z. Asghar, Numerical simulation of the peristaltic motion of a viscous fluid through a complex wavy non-uniform channel with magnetohydrodynamic effects. Phys. Scr. **94**, 115226 (2019)
56. K. Javid, M. Ellahi, K. Al-Khaled, M. Raza, S.U. Khan, M.I. Khan, E.R. El-Zahar, S. Gouadria, M. Afzaal, M.I. Khan, EMHD creeping rheology of nanofluid through a micro-channel via ciliated propulsion under porosity and thermal effects. Case Stud. Therm. Eng. **30**, 101746 (2022)
57. K. Javid, M. Hassan, D. Tripathi, S. Khan, E. Bobescu, M.M. Bhatti, Double-diffusion convective biomimetic flow of nanofluid in a complex divergent porous wavy medium under magnetic effects. J. Biol. Phys. **47**, 477 (2021)
58. S.J. Dèdèwanou, A.L. Hinvi, H.C. Miwadinou, A.V. Monwanou, J.B.C. Orou, Chaotic convection in a horizontal cavity filled with (alumina–copper)/water hybrid nanofluid heated from below in presence of magnetic field. Braz. J. Phys. **51**, 1079 (2021)
59. M.N. Aslam, A. Riaz, N. Shaukat, S. Ali, S. Akram, M.M. Bhatti, Analysis of incompressible viscous fluid flow in convergent and divergent channels with a hybrid metaheuristic optimization techniques in ANN: an intelligent approach. J. Cent. S. Univ. **30**, 4149 (2023)